ELSEVIER

Applied Surface Science 205 (2003) 231–239

applied surface science

www.elsevier.com/locate/apsusc

Extracting inter-diffusion parameters of TiC from AES depth profiles

H.C. Swart*, A.J. Jonker, C.H. Claassens, R. Chen, L.A. Venter, P. Ramoshebe, E. Wurth, J.J. Terblans, W.D. Roos

Department of Physics, University of the Free-State, P.O. Box 339, Bloemfontein ZA9300, South Africa

Received 7 August 2002; received in revised form 18 September 2002; accepted 18 September 2002

Abstract

The excellent corrosion and wear resistance of titanium carbide gives it a wide range of technological applications. Thin layers Ti (2300 Å) and C (2020 Å), were deposited onto SiO_2/Si substrates by means of electron beam evaporation in high vacuum. These films were annealed at different temperatures and times (temperatures ranging between 525 and 625 °C and annealing times between 4 and 121 min) to grow thin films of TiC. Ar^+ sputter depth profiling, with Auger electron spectroscopy (AES), provided the depth composition of the annealed films. A comparison between AES spectra of C in the graphite and carbide chemical states showed significant differences in both shape and energy of the differentiated peaks. A positive restricted linear least squares (PRLLS) method was used to separate the graphite and carbide contributions from the C profile. The TiC layer thickness for each specimen was obtained. With known TiC thickness and annealing times, the diffusion coefficients as a function of temperature were calculated. An Arrhenius plot yielded an activation energy Q of 207 ± 4 kJ/mol and a pre-exponential factor D_0 of 4.1×10^{-8} m^2 s^{-1}.
© 2002 Elsevier Science B.V. All rights reserved.

Keywords: TiC; PRLLS; Diffusion; AES; Activation energy

1. Introduction

Transition-metal carbides and nitrides are widely used as wear resistant coatings for cutting tools and bearing surfaces [1]. The bonding in this inter-metallic compound is mainly covalent [2], resulting in an exceptionally hard material with wide applications in corrosion and wear protection. TiC is a promising material due to its good high temperature strength and hardness. Its thermal and electrical properties made it ideal for semiconductor applications. These properties are highly dependent on stoichiometry, which is difficult to evaluate with Auger electron spectroscopy (AES). C atoms occupy the tetrahedral vacancies of the close-packed metal crystal when reacting with transition metals such as Ti. These carbides are generally very hard materials with high melting points, which makes it suitable for use in turbine engines. Recently, Ti has also been used in fittings for prosthetic devices, artificial hearts and other surgical implants. The combination of C and Ti enhances the properties of the Ti resulting in a compound that is used extensively in industry as a coating material. The interaction of metal layers with C is of interest for many applications

* Corresponding author. Tel.: +27-51-401-2926; fax: +27-51-401-3507.
E-mail address: swarthc@sci.uovs.ac.za (H.C. Swart).

0169-4332/02/$ – see front matter © 2002 Elsevier Science B.V. All rights reserved.
PII: S0169-4332(02)01070-X

in technology. Thermo-mechanical stability, electrical contact and erosion resistance depend on the inter-diffusion of these materials and the ability of the metal to form a carbide interlayer. In thermonuclear experiments, metal doping of graphite is considered for reducing the chemical erosion of C in the presence of hydrogen plasma ions due to hydrocarbon formation. The suitability of the metal doping will depend on the reactivity with C atoms. Ti is one of the metal dopings where large reduction of the chemical erosion of graphite by hydrogen ions was observed.

The rate of TiC growth mainly depends on the diffusion of C through the TiC [3] according to a study done on the effect of different C sources on the combustion synthesis of TiC. It was found that the rate of diffusion of Ti through TiC was four orders slower than that of C diffusing through the TiC. The activation energy for C and Ti diffusion through solid TiC were found to be in the range of 234–410 kJ/mol (C) and 738 kJ/mol (Ti), respectively, depending on the method of measurement [3]. Albertsen and Schaller [4] determined the diffusion coefficient in the temperature range of 1170–2413 K. Diffusion of C in TiC was investigated over the entire phase field using suitably designed diffusion couples. The diffusion exhibited a strong concentration dependence above 1468 K. The thermodynamic factor obtained from a thermodynamic analysis of the TiC system was used to describe the concentration dependence. Tracer diffusion coefficients were calculated from the chemical diffusion coefficients with the help of the thermodynamic factor. Below 1468 K concentration-independent diffusion coefficients were obtained which yielded a lower energy of activation of 174 kJ/mol. This behavior is attributed to the preponderance of grain boundary diffusion over volume diffusion at low temperatures in the samples at hand.

AES depth profiling measures the intensities in a specified energy range and calculates the maximum peak-to-peak height as function of sputtering time. This procedure can be done for several energy ranges (elements) to construct a traditional depth profile. These AES depth profiles are misleading when peak shape changes occur, due to a change in chemical environment. In the last two decades, the C KLL Auger peak shape has been measured and extensively used to determine the chemical state of C on solid surfaces [5–7]. Most of the work was, however, of qualitative nature. The AES derivative mode spectrum from C is particularly sensitive to the type of bond hybridization. During the formation of TiC, C undergoes a transition from an sp^2 hybridization (graphite) state to an sp^3 hybridization (carbide) state. Due to the superposition of the C Auger peak of graphite and the C Auger peak of TiC the signals cannot be monitored separately during Auger peak-to-peak height (APPH) measurements. One method that can be used successfully to obtain chemical information from the depth profiles is a linear least squares method [8,9]. This paper is devoted to extract the TiC thickness that formed during the annealing of thin Ti/C layers, by using AES. The inter-diffusion parameters for the TiC system were determined from the TiC thickness grown at different annealing times and temperatures. The inter-diffusion parameters of interest are the diffusion coefficients D, as a function of temperature, the pre-exponential factor D_0 and the activation energy Q.

2. Experimental

SiO_2 substrates with a thickness of 4000 Å were prepared by thermal oxidation of Si(1 0 0) wafers in a wet oxygen atmosphere for 1 h at a temperature of 1000 °C. Prior to the oxidation, the Si wafers were cleaned ultrasonically in acetone. This was followed by evaporating thin layers of Ti and C, onto the substrate by means of electron beam evaporation. Ti was evaporated first in order to limit surface contamination by eliminating the gettering effect of Ti. The evaporating of the films were done in a bell jar evaporation system with a pressure between 10^{-7} and 10^{-8} Torr and an electron beam current of between 100 and 350 mA. A calibrated Inficon thickness monitor was used to determine the thickness of the thin layers during evaporation. The samples were then cut into 5 mm × 5 mm squares and annealed in a tube furnace with a base pressure of $\leq 5 \times 10^{-7}$ Torr. A summary of the annealing times and temperatures for the different samples is shown in Table 1.

The samples were then subjected to Auger electron spectroscopy. The Auger measurements were done in a Computerized Physical Electronics, PHI 590 Model, Auger spectrometer equipped with a cylindrical mirror analyzer (CMA) and a 10 keV co-axial electron gun. The base pressure in the AES system was

Table 1
Annealing times and temperatures for the different samples.

Temperature (°C)	Annealing time (min)				
550	25	49	81	121	–
575	4	16	25	49	81
600	4	16	25	49	81
625	4	25	49	–	–

less than 1×10^{-9} Torr. Auger electrons were excited with a 3 keV energy primary electron beam having a current of 3.4 μA. A modulation voltage of 2 V on the CMA and a multiplier voltage of 1.4 kV was used. A 3 keV Ar^+ ion beam with a ion current density of 0.751 A m^{-2} was restored over an area of 3 mm × 3 mm to obtain the depth profiles. For each specimen, APPH versus time for Si (71–103 eV), C (230–310 eV), Ti (340–460 eV) and O (460–530 eV) were measured. All the peak shapes were saved during sputtering. A spectrum representing pure graphite and another representing the pure carbide was used as standards. The C peak shapes were fitted with a series of linear combinations of the standards. A linear least square fit was used to construct the depth profiles of the graphite and carbide.

3. Results and discussion

The elemental sputter rate for graphite and Ti was experimentally determined by depth profiling of unannealed samples with accurately known thickness of Ti and C thin layers. Fig. 1 is a APPH depth profile of the unannealed sample (**A** indicates when the sputtering was started.). The thickness for C and Ti, as evaporated, were 2296 and 2020 Å, respectively. The apparent broadening of the interface in Fig. 1 is the result of the escape depth of the Auger electrons and due to collisional mixing caused by the ion beam. Thus, C atoms are not only sputtered from the surface, but also knocked into the Ti layer by the primary ion beam [10]. Other effects that may be responsible for the degradation of this depth profile include ion-induced surface topography, preferential sputtering, ion implantation and diffusion due to electron beam heating [11]. The sputter time that represents the end of the C layer is taken at 50% of full height of the normalized APPH. The full width at half maximum (FWHM) of the normalized Ti concentration is indicative of the time to sputter through the Ti layer. With the known sputter times and thickness, the elemental sputter rates were calculated. Using these values, the sputter rates

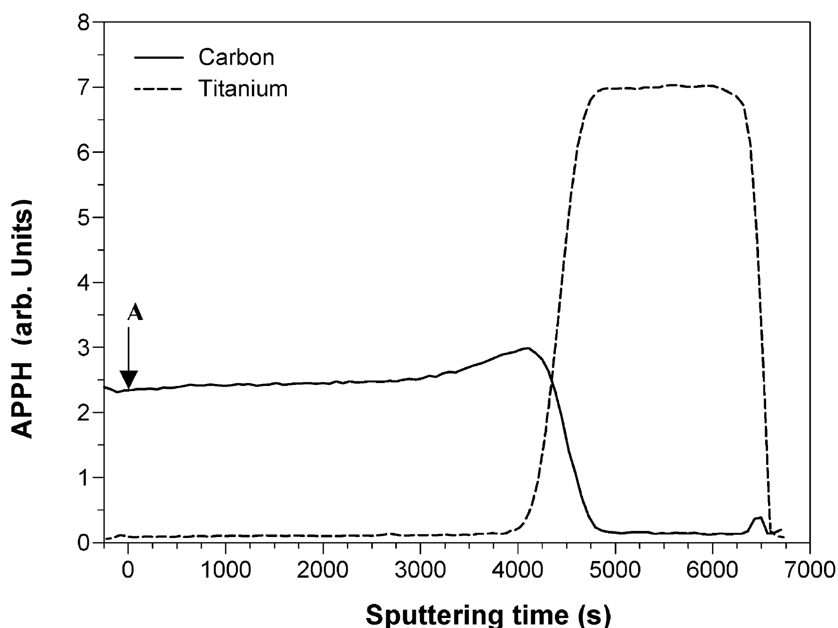

Fig. 1. Depth profile of an unannealed sample sputtered with an ion beam with a current density of 0.751 A m^{-2}.

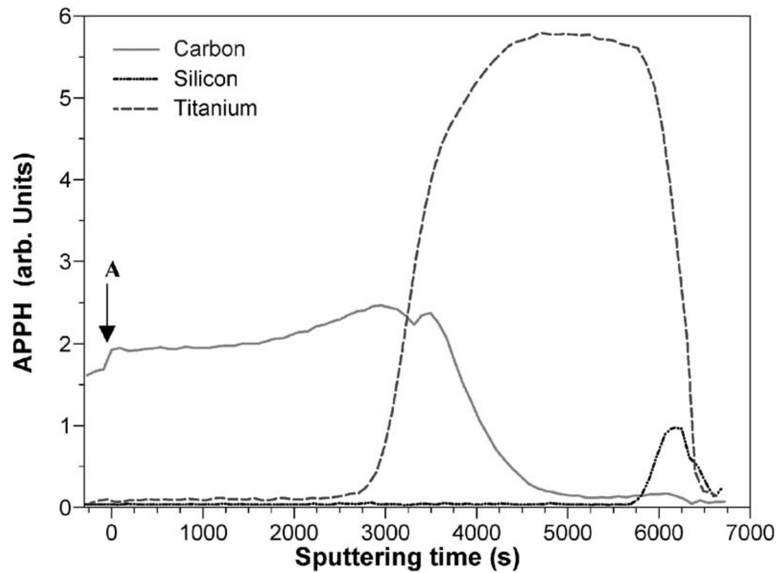

Fig. 2. Graph of APPH vs. time for a specimen annealed at 550 °C for 121 min.

for C, in the graphite form, and Ti, as a pure metal, were calculated to be $\dot{z}_{C} = 0.48$ Å s^{-1} and $\dot{z}_{Ti} = 0.97$ Å s^{-1}. Another important feature resulting from Fig. 1 is the apparent increase in concentration of C near the interface. This is due to the higher yield of backscattered electrons from the heavier Ti atoms near the interface, which result in the excitation of more Auger electrons in the C layer than usual.

A graph of APPH versus time for the specimen annealed at 550 °C for 121 min is illustrated in Fig. 2. The normalized depth profile (the profile was normalized to the maximum value of the C and the Ti APPH's) for the specimen annealed for 121 min at 550 °C is shown in Fig. 3. (*Note*: The data before sputtering was started is removed.) From the shape of the C curve, that was measured, at the interface, it was evident that a compound was formed, in this case TiC. A comparison between the AES spectra for C in the C–C bonding state (graphite) and C as carbide in the C–Ti bonding state is made in Fig. 4. It is clear from the fine structure of the two spectra that a significant difference exists between the two chemical states of the C. The Auger peak shape of C and associated fine structure change markedly from graphite to carbide. The peak shapes are similar to spectra already described in the literature [12,13]. There is also a slight shift in the peak position. The change in energy of the C KVV peak changing from graphite to carbide was measured to be 0.5 eV. This result correlates with the findings of Maline et al. [14] who illustrated that the C KVV non-differentiated peak shifts from 267 eV for the C–C bonding state to 269 eV in the C–Ti bonding state.

In order to determine the thickness of the formed TiC films accurately, it is necessary to know the carbide contributions to the measured C APPH values in the depth profiles. As shown in Fig. 4, there is a close overlap of the peaks of the two chemical states of C. This close overlap causes a superposition of the C Auger peak of graphite and the C Auger peak of carbide, which implies that the two peaks cannot be monitored separately with conventional APPH measurements. A positive restricted linear least squares (PRLLS) method was used to determine the fraction that pure graphite and pure carbide contribute to each point in the depth profile. This method makes use of standard C Auger spectra of graphite and carbide to determine the contribution of each to a measured Auger spectrum from a specimen containing both chemical states of C.

Let $\boldsymbol{a}_1$ and $\boldsymbol{a}_2$ be two $N \times 1$ vectors containing the spectra of the graphite and carbide standards, respec-

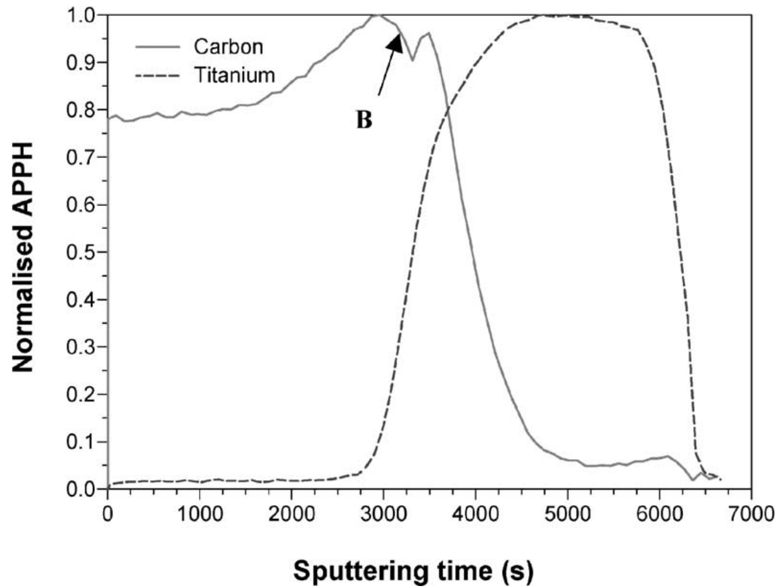

Fig. 3. Normalized depth profile for a specimen annealed for 121 min at 550 °C.

tively. The $N \times 2$ matrix, $\boldsymbol{A} = [\boldsymbol{a}_1, \boldsymbol{a}_2]$ is constructed. Let each measured spectrum $\boldsymbol{B}$, be an $N \times 1$ vector containing the Auger spectrum of the combination of graphite and carbide.

The 2×1 vector $\boldsymbol{X} = [\boldsymbol{x}_1, \boldsymbol{x}_2]$, with $\boldsymbol{x}_1$ and $\boldsymbol{x}_2$ being the fractions of $\boldsymbol{a}_1$ and $\boldsymbol{a}_2$ in $\boldsymbol{B}$, is the least squares solution to the over-determined system:

$$\boldsymbol{AX} = \boldsymbol{B} \tag{1}$$

given by [8,9].

$$\boldsymbol{X} = (\boldsymbol{A}^{\mathrm{T}}\boldsymbol{A})^{-1}\boldsymbol{A}^{\mathrm{T}}\boldsymbol{B} \tag{2}$$

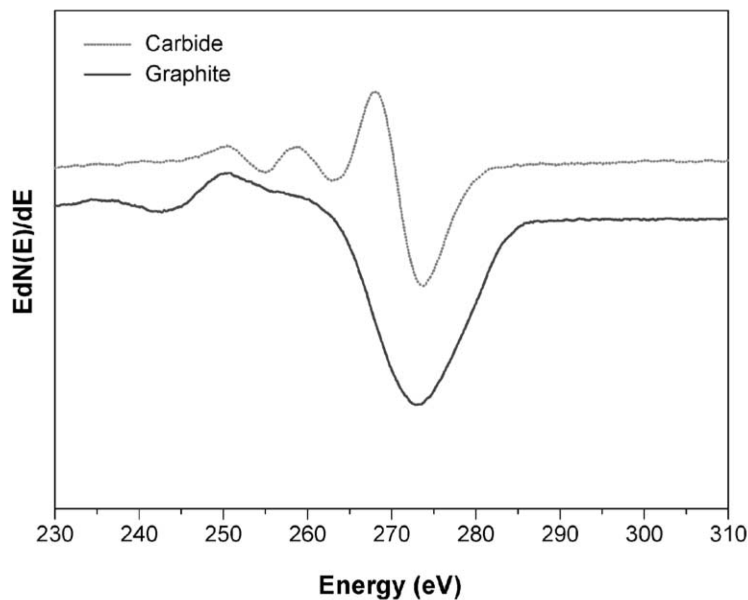

Fig. 4. C Auger standard spectra for graphite and carbide in TiC.

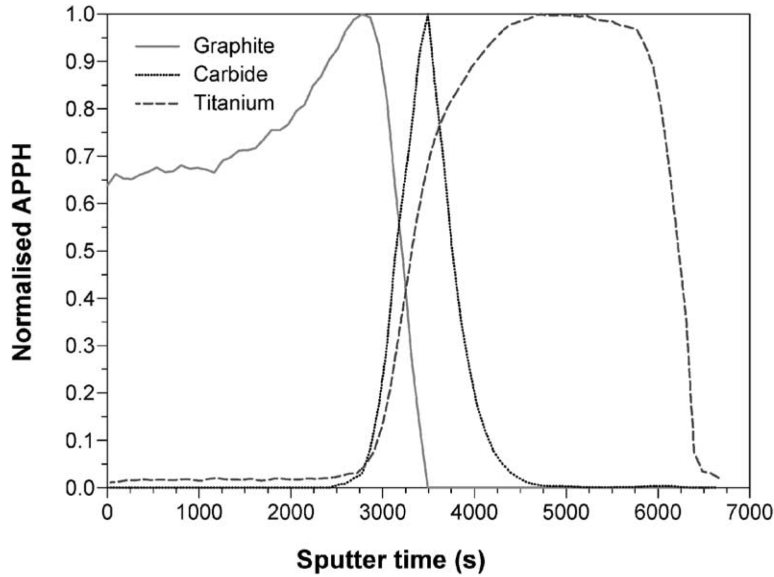

Fig. 5. Resolved carbide and graphite normalized APPH.

In addition to the over-determined system (1), consider two over-determined systems:

$$\boldsymbol{a}_1 y_1 = \boldsymbol{B}$$

and

$$\boldsymbol{a}_2 y_2 = \boldsymbol{B}$$

which have linear least squares solutions

$$y_1 = \frac{\boldsymbol{a}_1^{\mathrm{T}}\boldsymbol{B}}{\boldsymbol{a}_1^{\mathrm{T}}\boldsymbol{a}_1}$$

and

$$y_2 = \frac{\boldsymbol{a}_2^{\mathrm{T}}\boldsymbol{B}}{\boldsymbol{a}_2^{\mathrm{T}}\boldsymbol{a}_2}$$

The PRLLS technique takes into account the fact that the fractions can turn out to be negative if the atomic percentage of either graphite or carbide is very small, or if the overall C peak is small and partially buried in the background noise. The PRLLS solution $\boldsymbol{Z}$ is given by:

$$\boldsymbol{Z} = \begin{cases} [\boldsymbol{X}], & \text{if both } x_1 \text{ and } x_2 \text{ are positive} \\ \begin{bmatrix} 0 \\ y_2 \end{bmatrix}, & \text{if } x_1 \text{ is negative} \\ \begin{bmatrix} y_1 \\ 0 \end{bmatrix}, & \text{if } x_2 \text{ is negative} \\ \begin{bmatrix} 0 \\ 0 \end{bmatrix}, & \text{if both } x_1 \text{ and } x_2 \text{ are negative} \end{cases} \tag{3}$$

Physically, y_1 can be considered as the amount of graphite in the spectrum assuming there is no carbide, and y_2 as the amount of carbide without any graphite present. This solution gives the fractions of the graphite and carbide peaks present at a certain depth. PRLLS was used to solve the above-mentioned equations for each set of samples.

The results of the PRLLS method applied to each data set in the depth profile of Fig. 3 is illustrated in Fig. 5. To illustrate the accuracy of the PRLLS technique, Eq. (2) was used to reconstruct the C Auger spectrum at an arbitrary point **B** in Fig. 3. The reconstructed spectrum is compared with the measured spectrum in Fig. 6. It must be pointed out that sputtering of binary alloys [15] may lead to subsurface modification of the concentration profile and was not taken into account during this study. With the graphite and carbide contributions in the depth profile separated, it is possible to determine the thickness of the TiC layer by converting the time axis to a depth scale. The depth scale was determined by using the experimentally determined sputter rates of graphite and Ti (sputter rate = thickness/sputter time) for the two regions of the depth profile of the unannealed sample where there were assumable only pure elements present. In the interface, which contains TiC of variable stoichiometry the sputter rate, $\dot{z}_{\mathrm{TiC}}(t)$, were calculated

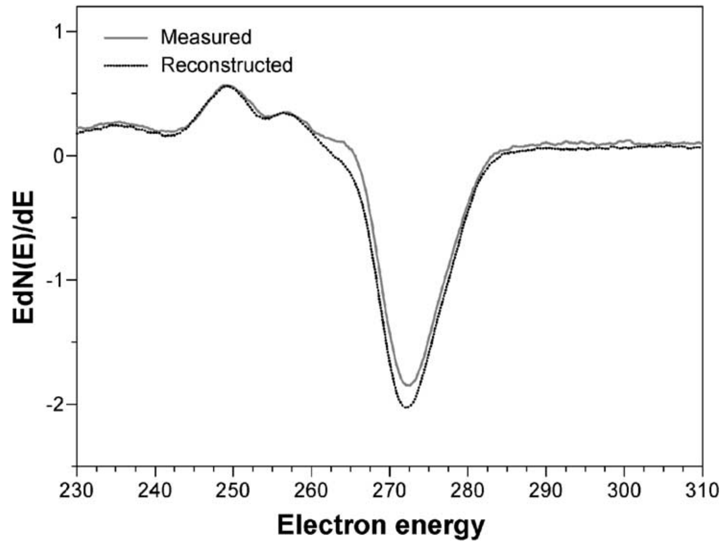

Fig. 6. Auger spectrum to compare measured data with data reconstructed using the PRLLS method.

using the first order approximation:

$$\dot{z}_{\mathrm{TiC}}(t) = x_{\mathrm{C}}(t)\dot{z}_{\mathrm{C}} + x_{\mathrm{Ti}}(t)\dot{z}_{\mathrm{Ti}} \tag{4}$$

with x_{C} and x_{Ti} being the fractions of the normalized APPH's of C and Ti, respectively. Summation of the TiC thickness over each time interval resulted in the total thickness of the interface. The actual thickness of the TiC layer was taken as the FWHM of the carbide portion of the depth profile. If the width of the compound layer is diffusion limited then the diffusion distance x is time dependent to the power of one-half, with the square root of the diffusion coefficient, $D^{1/2}$,

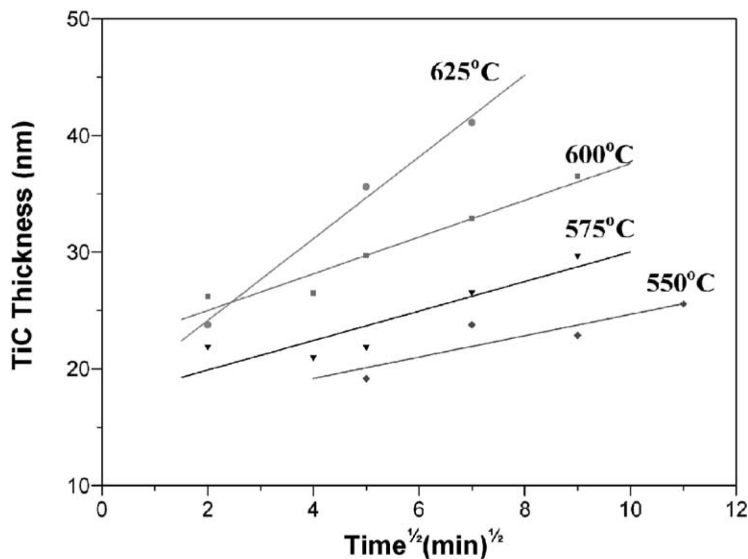

Fig. 7. Carbide thickness as a function of annealing time and temperature.

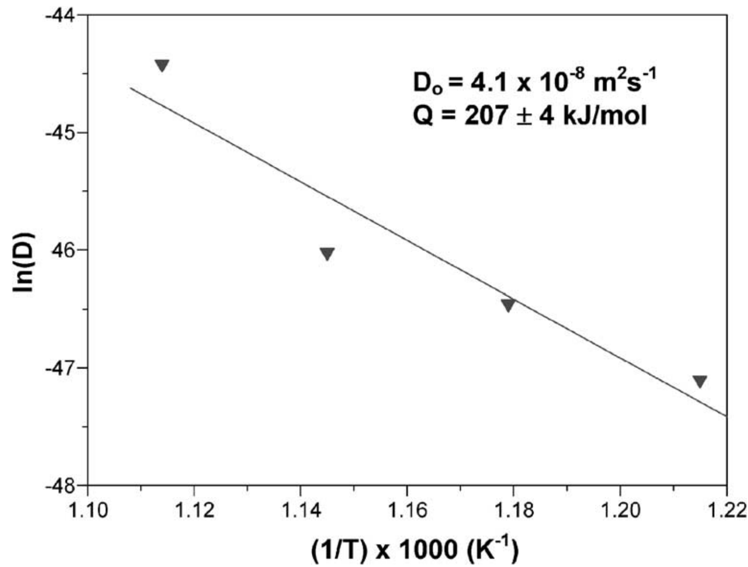

Fig. 8. Arrhenius plot.

being incorporated into the equation:

$$x = \sqrt{4Dt} \qquad (5)$$

For each temperature, the carbide thickness was plotted versus the square root of annealing time (see Fig. 7). The thickness is not zero for time zero as required by Eq. (5) due to the experimental error incorporated in the process of determining the carbide thickness. The error is mainly due to the broadening effect of the interface due to the ion beam. The relative increase of the carbide thickness for longer times at the different temperatures however, would not be dramatically influenced by the ion beam. The slopes of the thickness versus the square root of annealing time would therefore not change due to the broadening effect. There were also some minor signs of carbide formation at the interface of the unannealed samples, which might be due to the C/Ti intermixing of the first few atomic layers during evaporation and/or due to the ion beam mixing during sputtering through the interface.

The slopes in Fig. 7 are equal to $2D^{1/2}$, from which the diffusion coefficients were calculated. The interdiffusion parameters of interest are the diffusion coefficients D as a function of temperatures, the pre-exponential factor D_0 for the diffusion system as well as the activation energy Q. The latter two quantities can be determined from an Arrhenius plot [16].

The diffusion coefficient ($D_0 = 4.1 \times 10^{-8}\ \text{m}^2\ \text{s}^{-1}$) is obtained from the y-intercept of the Arrhenius plot and the activation energy ($Q = 207 \pm 4$ kJ/mol) from the slope of the plot, as illustrated in Fig. 8. These values are in agreement with previous results [4], where C was found to be the dominant diffusion specie.

4. Conclusion

Depth profiling, using AES, revealed significant amounts of TiC formed when adjacent thin films of Ti and C were annealed at temperatures ranging from 550 to 625 °C for time intervals of 4–121 min. Besides a change in the shape of the C differentiated AES peak, going from graphite to carbide, a shift of 0.5 eV towards higher energy was also observed. An increase in carbide thickness with increasing annealing time was measured at all temperatures. Diffusion coefficients were calculated from the slopes of these curves. An activation energy of 207 ± 4 kJ/mol that was determined in this study falls in the range of values previously determined.

References

[1] B. Wendler, K. Jakubowski, J. Vac. Sci. Technol. A 6 (1) (1988) 93.

[2] A. Shröer, W. Ensinger, Surf. Coat. Technol. 84 (1996) 448.

[3] Y. Choi, S. Rhee, J. Mater. Sci. 30 (1995) 4637.

[4] K. Albertsen, H. Schaller, Phys. Chem. 98 (1994) 1224.

[5] M.P. Seah, J.C. Rivière, in: D. Briggs, M.P. Seah (Eds.), Practical Surface Analysis, vol. 1, Auger and X-ray Photoelectron Spectroscopy, Wiley, New York, 1990, p. 102.

[6] W.S.M. Werner, P.J.M. Schmölz, H.W. Wagner, H. Störi, J. Kiefer, Surf. Interface Anal. 26 (1998) 590.

[7] A. Steiner, U. Falke, Surf. Interface Anal. 23 (1995) 789.

[8] W.D. Roos, G.N. van Wyk, J. du Plessis, Surf. Interface Anal. 22 (1994) 65.

[9] H. Anton, C. Rorres, Elementary Linear Algebra, Wiley, New York, 1994, p. 331.

[10] S. Hofmann, in: D. Briggs, M.P. Seah (Eds.), Practical Surface Analysis, vol. 1, Auger and X-ray Photoelectron Spectroscopy, Wiley, New York, 1990, p. 156.

[11] H.E. Bishop, in: J.M. Walls (Ed.), Methods of Surface Analysis, Cambridge University Press, Cambridge, 1989, p. 87.

[12] W.F. Stickle, D.G. Watson, J. Vac. Sci. Technol. A 10 (4) (1992) 2806.

[13] W.F. Stickle, D.G. Watson, J.F. Moulder, J. Vac. Sci. Technol. A 8 (3) (1990) 2217.

[14] M. Maline, M. Ducarroir, F. Teyssandier, R. Hillel, R. Berjoan, F.J.J. Van Loo, W. Wakelkamp, Surf. Sci. 286 (1993) 82.

[15] R. Kelly, Nucl. Instr. Meth. B39 (1989) 43.

[16] D.R. Askeland, The Science and Engineering of Materials, Stanley Thornes Publishers Ltd., Cheltenham, 1998, p. 120.